GEOFLUIDS
Geofluids (2011) 11, 309–327 doi: 10.1111/j.1468-8123.2011.00342.x

# The relevance of vein texture in understanding the past hydraulic behaviour of a crystalline rock mass: reconstruction of the palaeohydrology of the Mecsekalja Zone, south Hungary

G. DABI[1], Z. SIKLÓSY[2], F. SCHUBERT[1], B. BAJNÓCZI[2] AND T. M. TÓTH[1]

[1]*Department of Mineralogy, Geochemistry and Petrology, University of Szeged, Szeged, Hungary;* [2]*Institute for Geochemical Research, Hungarian Academy of Sciences, Budapest, Hungary*

## ABSTRACT

This study reconstructs the palaeohydrogeologic evolution of the shallow-to-moderate Mesozoic subsidence history for the Mecsekalja Zone (MZ), a narrow metamorphic belt in the eastern Mecsek Mountains, Hungary. Brittle deformation of the MZ produced a vein system with a cement history consisting of five sequential carbonate generations and one quartz phase. Vein textures suggest different fluid-flow mechanisms for the parent fluids of subsequent cement generations. Combined microthermometric and stable-isotope measurements permit reconstruction of the character of subsequent fluid generations with different flow types, as defined by vein textures, yielding new information regarding the hydraulic behaviour of a metamorphic crystalline complex. Textural observations and geochemical data suggest that fracture-controlled flow pathways and externally derived fluids were typical of some flow events, while percolation through the rock matrix and the relationship to the Cretaceous volcanism and dyke emplacement were typical of others. The difference in the mode of calcite deposition from pervasive fluids (i.e. pervasive carbonatisation along grain boundaries versus deposition in antitaxial veins) between two calcite generations related to the volcanism inspired a stress-dependent model of antitaxial vein growth. Textural and isotope variations in a vein generation produced by the same parent fluid indicate rock-dependent hydraulic behaviour for different rock types, distinct action of the contemporaneous fracture systems and different extents of fluid–rock interaction. Cathodoluminescence microscopy and fluid-inclusion microthermometry shed light on the possible role of hydraulic fracturing in the formation of massive calcite. The time of formation was estimated from the isotope composition of the oldest calcite generation and its presumptive relationship with the sedimentary sequences to the north, whereas microthermometry permitted conciliation of the reconstructed flow sequence with the Mesozoic subsidence history of the Mórágy Block (including the MZ).

Key words: microthermometry, palaeohydrogeology, stable isotopes, vein texture

Received 15 July 2010; accepted 20 June 2011

Corresponding author: Gergely Dabi, Department of Mineralogy, Geochemistry and Petrology, University of Szeged, Egyetem utca 2-6, 6722 Szeged, Hungary.
Email: dabi@geo.u-szeged.hu. Tel: +36 62 544 058. Fax: +36 62 426 479.

*Geofluids* (2011) 11, 309–327

## INTRODUCTION

Stable-isotope data are widely applied in palaeohydraulic reconstructions of hydrothermal vein systems in different geological settings. Applications include assessment of fluid–rock interaction (Hilgers & Sindern 2005) and the evolution of mineralising fluids during fluid–rock interaction (Cox 2007). Bottomley & Veizer (1992) and Rye & Bradbury (1988) assessed recrystallisation of a pre-existing vein system and fluid–rock interaction during nappe stacking, respectively. Templeton *et al.* (1998) investigated the mixing of mineralising fluids during compression-related fluid expulsion. Juhász *et al.* (2002) and Fourcade *et al.* (2002) used stable-isotope data, together with fluid-inclusion microthermometry, to resolve flow interactions between crystalline rocks and overlying sediments.

Numerous studies have proven the ability of stable isotopes to resolve the origins of fluids in crystalline rocks (e.g. Bottomley & Veizer 1992; Blyth *et al.* 2000).

In the recent decades, the formation of different vein textures and their implications for the flow regime (i.e. advective, fracture-channelised-flow versus percolation through the host rock) have been brought into focus (Bons 2000; Hilgers & Urai 2002a). Hilgers & Sindern (2005) and Barker *et al.* (2006) combined stable-isotope data with radiogenic isotopes ($Sr^{87}/Sr^{86}$) and trace and rare earth elements to resolve the fluid source and flow path of antitaxial vein parent fluids. Rye & Bradbury (1988) found that vein calcites with the same fluid source but different textures display different isotope compositions.

Deformation during the Mesozoic evolution of the Tisza Mega-unit (TMU) produced a postmetamorphic vein sequence in the Mecsekalja Zone (Dabi *et al.* 2009a), the only exposed representative of the TMU crystalline complexes. This study reports stable-isotope data in concert with a detailed textural description and fluid-inclusion microthermometry of veins from the Mecsekalja Zone (Mecsek Mountains, SW Hungary), to unravel the hydraulic behaviour of a metamorphic complex. The textural, isotope and microthermometric data are interpreted in with the context of the subsidence history of the Mecsekalja Zone and the well-known Mesozoic evolution of the Tisza Mega-unit, its wider environment. The palaeofluid evolution reconstructed from the vein sequence is synchronised with the postmetamorphic Alpine evolutionary stages of the Tisza Mega-unit and the Mesozoic subsidence history of the Mecsekalja Zone to yield new information about the tectonic conditions associated with different vein systems and textures.

## GEOLOGICAL BACKGROUND

The study area is representative of the metamorphic complexes of the Tisza Mega-unit (TMU), a large composite lithospheric block with complex internal structure made up of nappe systems (Fig. 1A, Kovács *et al.* 2000; Haas & Péró 2004). The TMU is the basement of the Pannonian Basin and is overlaid by thick Cenozoic sequences. Units of the TMU are built up of Variscan crystalline complexes beneath Upper Carboniferous to Triassic overstep sequences. Variscan granitoids and crystalline complexes of the TMU may be correlated with the Moldanubian (-Helvetic) Zone, which means that during the Variscan Orogeny the TMU was an integral part of the Variscan Mountain Range (Haas & Péró 2004) and thus, in its present position, the TMU is an exotic terrane of European Plate origin. Its Alpine evolutionary stages include Bathonian separation from the European Plate (because of the opening of the Penninic-Vahic ocean branch), Cretaceous continental rift-type alkali basalt volcanism and Late Cretaceous nappe stacking (Haas & Péró 2004). The main nappe-stacking stage was in the Turonian-Coniacian (pre-Gosau phase).

The Mecsekalja Zone (MZ) is a 1.5-km-wide, NE–SW-trending tectonic zone located in the Eastern Mecsek

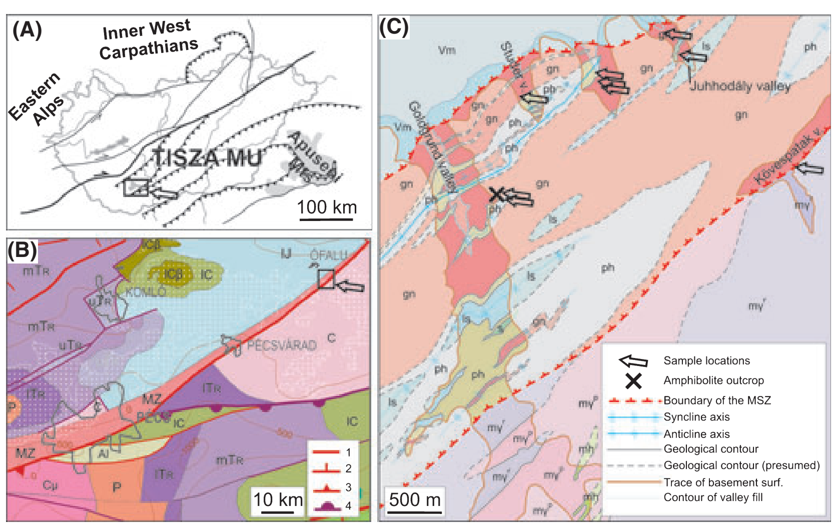


**Fig. 1.** (A) Position of the Tisza Mega-unit in the basement of the Pannonian Basin. Inset shows the position of B. (B) Regional geological map of the study area. The MZ is a narrow metamorphic zone between Mesozoic sequences in the Eastern Mecsek Mountains and the Variscan Mórágy Granite, Mórágy Hills. The contact of the MZ is tectonic both to the north and to the south. Dotted area marks surface outcrops of the pre-Cenozoic formations. 1. Cenozoic tectonic line, 2. Cenozoic fault, 3. Cenozoic overthrust, 4. Mesozoic nappe. Inset shows the position of C. (C) Outcrops of the MZ are exposed in the north–south valleys south-east of Ófalu village. The studied amphibolite body is marked with an X. Cμ, Variscan metamorphic complex; MZ, Mecsekalja Zone; C, Variscan granitoid rocks; P, Permian; lTR, Lower Triassic; mTR, Middle Triassic; uTR, Upper Triassic to Lower Jurassic; lJ, Lower to Middle Jurassic; lC, Upper Jurassic to Lower Cretaceous; lCβ, Lower Cretaceous basaltic rocks; Al, Albian; gn, gneiss; ph, phyllite; s, serpentinite; ls, limestone; m$\gamma^r$, rarely porphyritic monzogranite; m$\gamma^p$, porphyritic monzogranite; mh, monzonite; Vm, Vasas Marl Formation. After Balla *et al.* 2009.

Mountains, Hungary (Fig. 1B), which can be traced in boreholes to the north-east under a thick cover of overlying Cenozoic to Quaternary sediments (Fülöp 1994). At the study area, the zone is composed of enclaves of amphibolites (originally not marked on the cited map), serpentinite and crystalline limestone bodies in host mylonitic gneiss and quartz phyllite (Balla *et al.* 2009; Fig 1C). The amphibolite was metamorphosed at 580°C and a pressure between 2 and 4 kbar (Árkai & Nagy 1994), whereas the peak metamorphism of the host mylonitic gneiss is around 450°C and 6.7 to 7.3 kbar (Lelkes-Felvári *et al.* 2000). The age of mylonitic shearing has been dated to between 270 and 303 Ma (Lelkes-Felvári *et al.* 2000) by the K/Ar method. Based on zircon morphology, the protolith of the mylonite has been defined as granitic orthogneiss, the protolith of which crystallised at 710°C followed by metamorphic recrystallisation at 550°C (M. Tóth *et al.* 2005). The crystalline limestone bodies contain lower Devonian conodonts (S. Kovács, Eötvös University, oral communication, 2010). These rock types are referred collectively as the Ófalu Formation. Their common foliation suggests that they were metamorphosed and deformed together. Rocks of the Ófalu Formation are strongly foliated. The trend of their foliation is NE – SW, with a steep dip. The common foliation and lack of brittle deformation along their boundaries suggest a common history during the Late Carboniferous to Early Permian mylonitic shearing of the gneiss, along its retrograde path. Dabi *et al.* (2009a) described a six-phase vein evolution from the Goldgrund valley amphibolite body, and Dabi *et al.* (2009b) presented fluid-inclusion microthermometry from antitaxial veins crosscutting the gneissic rocks.

The MZ is bordered by tectonic contacts both north and south; the neighbouring rocks are Liassic marls (Vasas Marl Formation, Császár *et al.* 2007) and Variscan granites (Mórágy Granite Formation, Király & Koroknai 2003; Balla *et al.* 2009), respectively (Fig. 1B,C). The north-west boundary is a long-recognised structural line, although its character is not yet defined, with a dip angle between 35 and 50° to the north-west, according to coal exploration wells (Balla *et al.* 2009). The continuity of the sedimentary sequences to the north and their age (Carboniferous to Late Cretaceous) suggest that the present-day structure was formed later than Late Cretaceous. The geometry of the south-east boundary is less known; though, its tectonic character is presumptive based on brittle features at the contact zone and the lack of contact metamorphic features in the Ófalu Formation (Balla *et al.* 2009).

The Liassic marl to the north (Vasas Marl Formation) is a member of a continuous sedimentary sequence between the Upper Carboniferous and Upper Cretaceous (Fig. 1B). Marine sedimentation commenced in the Middle Triassic (Anisian Lapisi Limestone Formation) and continued until the Late Cretaceous, with pelagic marls and limestones between the Sinemurian and the Kimeridgian (Némedi Varga 1998). In the Eastern Mecsek Mountains, basaltic volcanism occurred in the Early Cretaceous between 135 and 110 Ma (Harangi 1994); though, volcanic bombs in the Late Berriasian and Hauterivian strata of the Márévár Limestone indicate an earlier initiation (ca. 140 Ma). Basaltic dykes are frequent in the study area and crosscut the rocks of the Mórágy Granite Formation, the Ófalu Formation and rocks of the Jurassic formations to the north. These rocks are referred to collectively as the Rozsdásserpenyő Alkaline Basalt Formation and are of alkali basaltic, alkali trachytic, to alkali rhyolitic composition (Balla *et al.* 2009). The dykes are possibly related to the basaltic volcanism in the eastern Mecsek Mountains, but their geochemical character suggests that they are more closely related to the subvolcanic rock types of the eastern Mecsek (Balla *et al.* 2009), which crosscut the folded structures of Cretaceous strata, implying an Upper Cretaceous age (Balla *et al.* 2009). Intrusive breccias frequently crosscut the rocks of the Mórágy Granite Formation and are regarded as the product of the enhanced volatile pressure during dyke emplacement (Balla *et al.* 2009). Pervasive carbonatisation and carbonate infiltration were described from rocks of the Mórágy Granite in the course of systematic petrographic investigations (Balla *et al.* 2009). The fine-grained carbonate usually forms thin 'films' around the single grains in

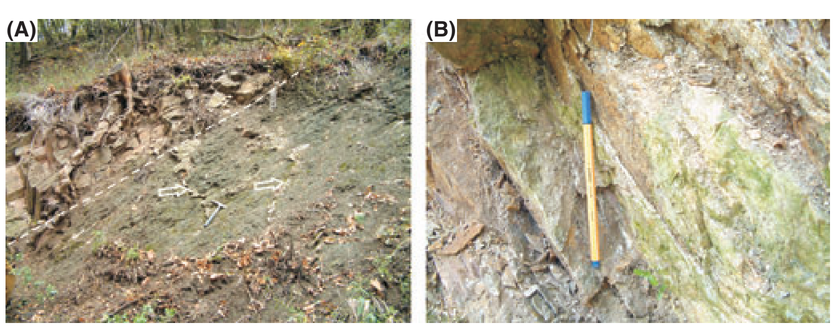


**Fig. 2.** Outcrop photographs. (A) Goldgrund valley amphibolite outcrop. The studied amphibolite body is marked with an X on Fig. 1C. The contact between the studied amphibolites and the host mylonitic gneiss is revealed by the outcrop. Veins are marked with arrows. (B) Juhhodály valley gneiss outcrop, with thin antitaxial vein at the pen-cap.

the granite. It is regarded as being 'triggered by the explosion-like escape of the volatile components' during dyke emplacement.

The Mórágy Granite to the south has been subject to a series of site investigations over the past decade as a potential location for a deep repository for low-level radioactive waste (for a summary see Balla *et al.* 2009). As part of these investigations, numerous studies of the palaeohydrogeology of the site were carried out, including analysis of the fluid-inclusion planes (FIPs) of rock-forming minerals and veins (Poros *et al.* 2008; Szabó *et al.* 2008). Szabó *et al.* (2008) identified four fluid-flow events. The fluids of a single regional event have homogenisation temperatures between 130 and 238°C, and salinities between 1.9% and 4.5% *w*NaCl equivalent. The remaining events were local. Two were of higher temperature and salinity (227°C < $T_h$ < 293°C, and 9.98–10.85% *w*NaCl equivalent respectively), and one was of lower temperature and salinity (137°C < $T_h$ < 209°C, 0.9–2.2% *w*NaCl equivalent, respectively). These fluid-flow events were defined based on the FIPs of rock-forming minerals, showing that the fluids of the regional event produced veining. Poros *et al.* (2008) defined six fluid-flow events, the fourth of which produced calcite veins and which they assigned to the regional flow event described by Szabó *et al.* (2008), based on its correspondingly low temperature and salinity ($T_h$ between 100 and 250°C, salinities between 0.2 and 5% *w*NaCl equivalent). Both Szabó *et al.* (2008) and Poros *et al.* (2008) observed regionally defined fluid flow in both the FIPs of rock-forming quartz and the primary inclusions of vein calcites. Poros *et al.* (2008) dated this regional flow event to the Late Cretaceous. Kovács-Pálffy & Földvári (2003) had previously published K/Ar age data of authigenic illites of veins which showed that the main period of veining was during the Mesozoic.

Császár (2003) constructed the Mesozoic subsidence curve of the Mórágy Block (including near-surface occurrences of the Mórágy Granite Formation and rocks of the Ófalu Formation) and the Jurassic Zsibrik Block to the north, where Jurassic sequences are exposed on and near the surface. These calculations suggest that Early to Late Cretaceous uplift of both blocks occurred because of the pre-Gosau tectonic movements. The study area is partially covered by Lower Miocene to Holocene sediments and loess.

## DESCRIPTION OF STUDIED VEINS

### Vein textures in amphibolite

The Goldgrund Valley outcrop (Figs 1C and 2A) provides an exceptionally good exposure of the amphibolite and permits study of a well-developed vein system. Dabi *et al.* (2009a) described a succession of five distinct carbonate and one quartz vein-filling phase which, based on their textures, define at least six fluid-circulation events (Fig. 3). The following section is a brief characterisation and interpretation of these vein textures.

The first vein-filling generation is syntaxial calcite consisting of white, intensely twinned elongate blocky crystals ($Cal_{EB}1$, Fig. 3A–C, Dabi *et al.* 2009a). $Cal_{EB}1$ makes up the majority of vein-filling minerals within the samples studied and evolved in at least two steps based on the braid-like configuration of the veins (Fig. 3B,C). Circulation of parent fluids ceased before the precipitated mineral completely filled the fractures, leaving closed voids in the centre (referred to as remnant voids, Fig. 3A,B). Vein occlusion in conjunction with a syntaxial texture is characteristic of advective transport and channelised flow (Lee *et al.* 1996; Hilgers & Urai 2002b; Hilgers *et al.* 2003). Cathodoluminescence image analysis reveals swarms of orange luminescent microveins (Fig. 4A) and red luminescent patches within adjacent crystals of elongate blocky calcite (Fig. 4B). $Cal_{EB}1$ calcite displays intense twinning. (G. Dabi, T. M. Tóth & F. Schubert, unpublished conference abstract, 2006) described latent oscillatory patterns subparallel with the crystal growth directions in the $Cal_{EB}1$ crystals, using UV-fluorescent microscopy.

Zoned dolomite ($Dol_{ZON}$) was precipitated in the closed remnant voids and grew syntaxially on pre-existing calcite scalenohedrons (Fig. 3D,E). Growth in these voids supposes percolation of parent fluids along a pre-existing vein system filled with $Cal_{EB}1$. Red luminescent patches, typical of dolomite, within the earlier vein calcite (Fig. 4B) further hint at percolation through the pre-existing vein system. These patches are interpreted to be indicative of metasomatic alteration of the pre-existing $Cal_{EB}1$ calcite along the percolation paths of the $Dol_{ZON}$ parent fluid. Cathodoluminescence image analysis reveals oscillatory subzones of the dolomite (Fig. 4C,D).

In the next phase of remnant void-filling, syntaxial blocky quartz was precipitated ($Qtz_{BL}$, Fig. 3D,E), the texture of which is characteristic of advective flow (Bons 2000; Hilgers & Urai 2002b; Hilgers *et al.* 2003). The presence of thin (~30 μm) microveins filled with quartz also suggests advective flow of the parent fluid, with quick occlusion of the flow pathways suggested by the sporadic occurrence of the blocky quartz.

Filling of remnant voids was completed with precipitation of a massive calcite (referred to as space-filling calcite, $Cal_{SF}$, Fig. 3D,E). Based on its orange luminescent colour (Fig. 4C,D) and the presence of swarms of orange cathodoluminescent microveins (Fig. 4A) transecting crystals of earlier elongate blocky calcite and zoned dolomite, its parent solution was associated with brecciation of the pre-existing vein system. This space-filling calcite displays less intense twinning than the preceding elongate blocky calcite.

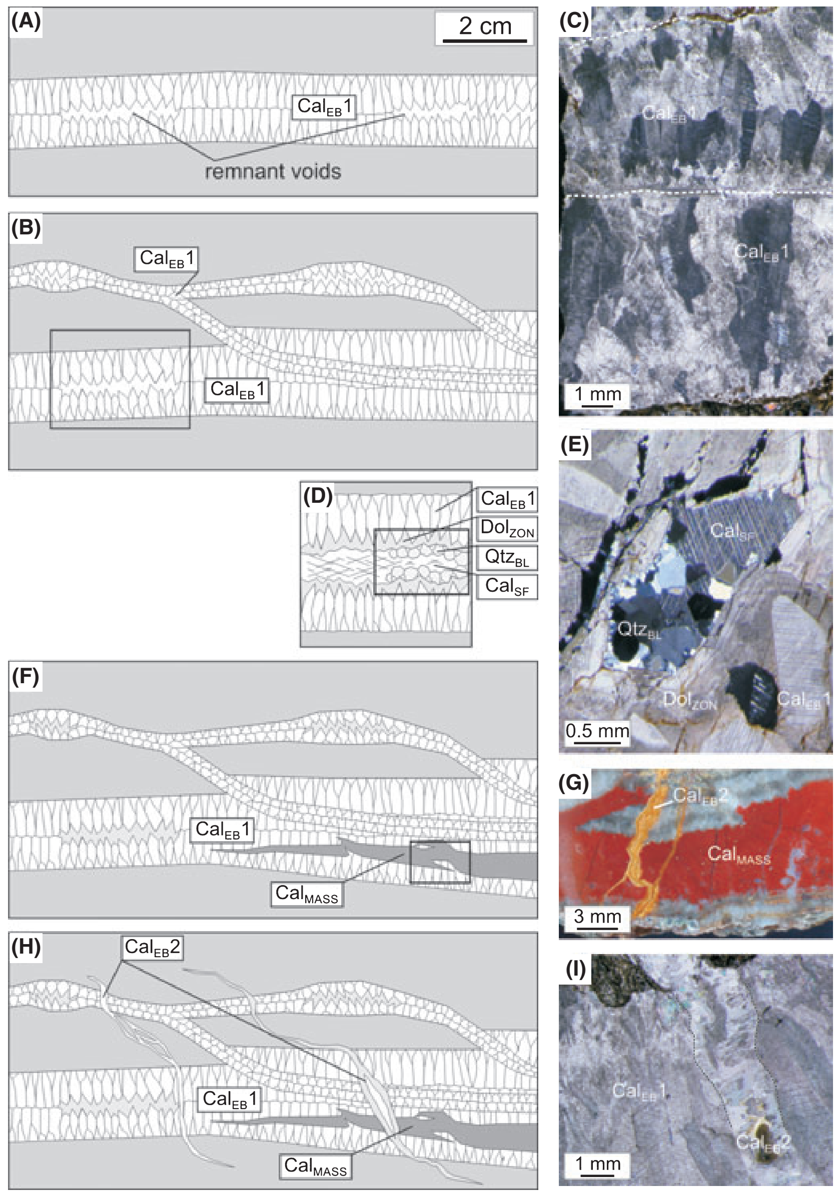


**Fig. 3.** The vein system in the studied amphibolite body (Dabi *et al.* 2009a). (A, B) Precipitation of $Cal_{EB}1$ occurred in at least two phases, based on the braid-like vein configurations. Remnant voids were present after occlusion of the vein system. (C) Vein filled with younger generation of $Cal_{EB}1$ (framed with dashed lines) cutting through an older vein of $Cal_{EB}1$. (D, E) Remnant voids are filled with zoned dolomite ($Dol_{ZON}$), blocky quartz ($Qtz_{BL}$) and massive space-filling calcite ($Cal_{SF}$). (F, G) Precipitation of the red massive calcite ($Cal_{MASS}$) owing to reopening of the vein system. Limonite-stained calcite ($Cal_{EB}2$) cuts through red massive calcite. (H, I) Late syntaxial calcite ($Cal_{EB}2$) cuts earlier phases.

In the next phase, reopening of the veins occurred and red, massive calcite was precipitated, containing solid inclusions of spherulitic haematite and quartz (referred to as massive calcite, $Cal_{MASS}$, Fig. 3F,G).

The above-described veins in the amphibolite body are transected by 2- to 3-mm-thick veins filled with elongate blocky calcite ($Cal_{EB}2$, Fig. 3H,I). These later veins display syntaxial growth and are either partly or entirely limonite stained (Fig. 3G) or white. In some places, bands of limonite-stained calcite and clear white calcite occur together in the same vein. In this case, yellow limonite-stained bands occur at the vein-wall interface, suggesting precipitation prior to the precipitation of the clear calcite (syntaxial growth). Both of these calcites are untwinned and lack any signs of subsequent alteration.

## Vein textures in mylonitic gneiss

Veins are prevalent in the mylonitic gneiss, although poor outcropping hinders exposure of mesoscale vein configurations. The outcrops from which samples were collected are represented in Fig. 1C.

Cathodoluminescence image analysis of the mylonitic gneiss revealed disseminated orange luminescent calcite in the rock matrix (Fig. 5A). Fourcade *et al.* (2002) ascribed disseminated carbonates as being precipitated from fluids that once pervaded the rock matrix. In the Mórágy Granite to the south, pervasive carbonatisation was ascribed to explosion-like escape of volatile components (Balla *et al.* 2009).

The mylonitic gneiss is generally cut by syntaxial elongate blocky calcite veins. These veins display intense twinning

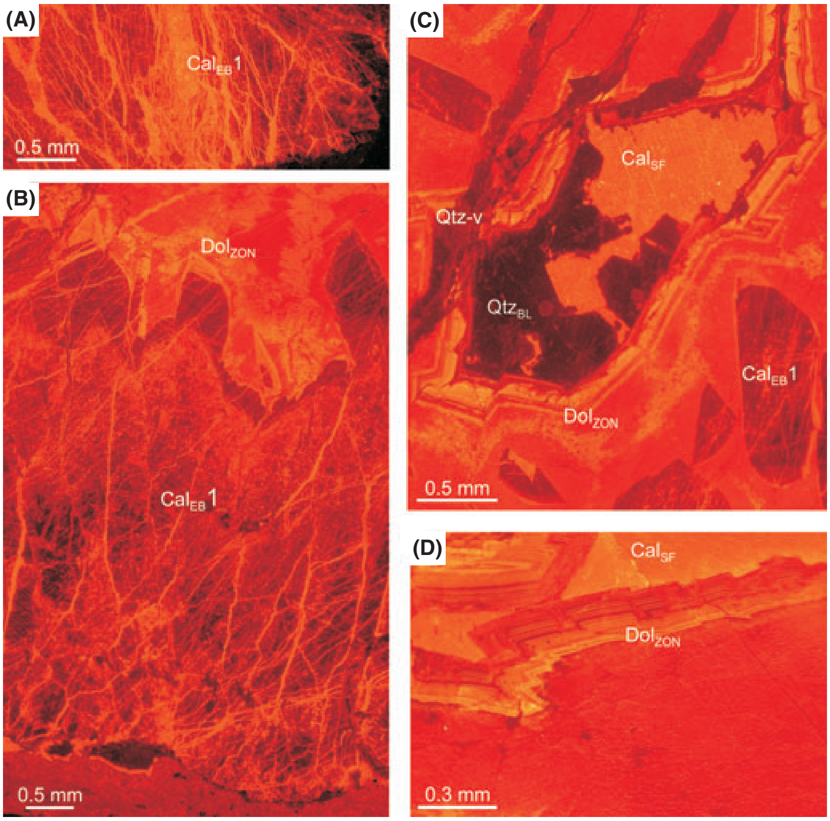


**Fig. 4.** Cathodoluminescence microscope images of the different textural types in the amphibolites cross-cutting veins. (A) Orange luminescent microvein swarm cutting through syntaxial calcite ($Cal_{EB}1$), displaying brecciation of the vein system. (B) Nonluminescent syntaxial calcite ($Cal_{EB}1$) and red luminescent zoned dolomite ($Dol_{ZON}$). Neighbouring crystals of $Cal_{EB}1$ are transected by red luminescent patches, suggesting percolation of a dolomitising fluid along the preceding vein system. Orange luminescent alteration of $Cal_{EB}1$ crystals along grain boundaries and in dolomite suggests pervasion of fluid from the vein-wall interface towards remnant voids. (C) Cathodoluminescence image of a remnant void segment with zoned dolomite ($Dol_{ZON}$), nonluminescent blocky quartz ($Qtz_{BL}$), veins filled with quartz (Qtz-v) and massive space-filling calcite ($Cal_{SF}$). (D) Oscillatory zonation in zoned dolomite ($Dol_{ZON}$).

(Fig. 5B) and in some places display faulted segments. Where present, remnant voids in the middle of veins contain dolomite. Cathodoluminescence images reveal intense alteration of these veins (Fig. 5C), with a high degree of twinning and alteration suggesting early precipitation of the calcite and a common origin with $Cal_{EB}1$.

Untwinned white antitaxial calcite veins ($Cal_{ANT}$) with a maximum width of ~5 mm are prevalent in the mylonitic gneiss (Fig. 2B). Dabi *et al.* (2009b) measured the homogenisation temperatures of primary fluid inclusions in the antitaxial veins. They found an extremely wide range of homogenisation temperatures (between 50 and 240°C), which they interpreted as caused by fluid-pressure fluctuation during vein development, and possibly stretching of the inclusions. The uniform salinities of the same inclusions, between 0.18 and 0.53% *w*NaCl equivalent, suggest a common origin. In some places, antitaxial veins constitute well-developed vein systems, but generally they are parallel with the foliation, implying that mechanic anisotropy of the rock (Twiss & Moores 1992) governed their formation. Calcite crystals in these veins display parallel (sometimes curved) grain boundaries or widen towards the vein-wall interface; that is, crystal boundaries diverge, suggesting growth competition (Bons 2000; Fig. 5D). The zones of divergent grain boundaries contain bands and trails of solid inclusions (Ramsay 1980; Hilgers & Urai 2005). All display characteristic signs of antitaxial growth (Hilgers *et al.* 2001). In some places, these veins contain a medial, yellow limonite-stained band (Fig. 5D), indicating that precipitation of limonite-stained calcite preceded precipitation of clear white calcite (antitaxial growth). This order of precipitation is consistent with that of the $Cal_{EB}2$ calcites and suggests their common origin. The parent fluids of veins displaying an antitaxial texture percolated through the host rock, according to Bons (2000), Hilgers & Urai (2002a) and Hilgers & Sindern (2005).

## METHODS

Fluid-inclusion studies were carried out at the Department of Mineralogy, Geochemistry and Petrology, University of Szeged, on a Linkam THMSG 600 heating-freezing stage mounted on an Olympus BX41 microscope. Doubly polished 60- to 70-μm-thick chips were first mapped for fluid inclusions. Initial heating of samples was carried out to avoid the stretching of inclusions resulting from freezing the aqueous liquid phase. Metastable equilibrium (lack of a vapour phase at temperatures of liquid and vapour coexistence) during cooling after homogenisation is common in studied inclusions. This inhibits $T_h$ measurements, especially at lower homogenisa-

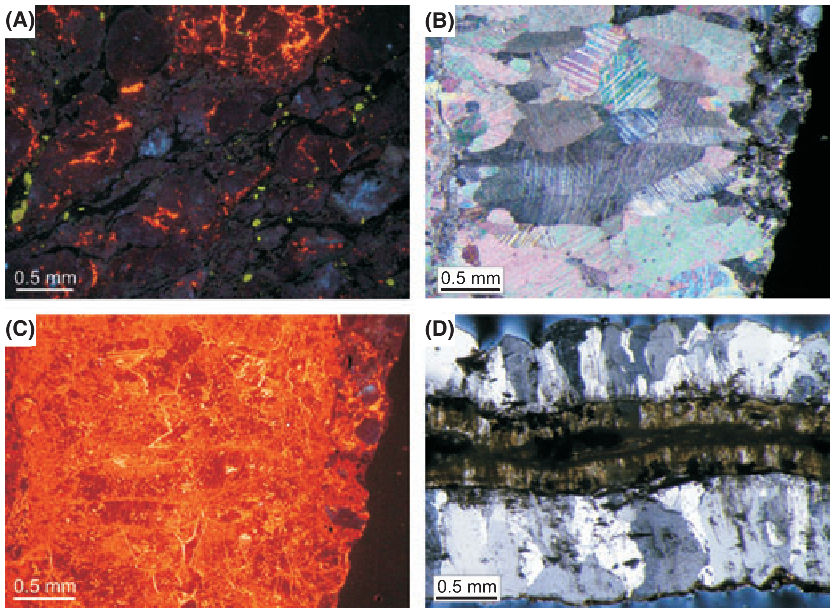


**Fig. 5.** Cathodoluminescence and optical microscope images of different calcite phases in the gneissic rocks. (A) Orange luminescent calcite seams in mylonitic gneiss (feldspars display bluish, apatites green luminescence colour). (B) Syntaxial elongate blocky calcite vein in mylonitic gneiss ($Cal_{EB}1$) displaying intense twinning. (C) Cathodoluminescence microscope image revealing intense alteration of the nonluminescent $Cal_{EB}1$. (D) Antitaxial vein in mylonitic gneiss. Band of limonite-stained calcite in the middle indicates that precipitation of limonite-stained calcite preceded that of the white clear calcite. Crystals widen towards the vein-wall interface and contain solid inclusion bands and trails dragged from the wall rock, indicating antitaxial growth.

tion temperatures (if homogenisation temperatures of inclusions are measured separately). Stepwise 1°C heating was applied, checking all studied inclusions between steps both to avoid the loss of the vapour phase before homogenisation temperature measurement and to avoid stretching of inclusions at lower homogenisation temperatures. Final melting temperature measurements were undertaken via the cycling technique (Goldstein & Reynolds 1994). Salinities are given according to Bodnar (1992). Calibration of the heating-freezing stage was carried out using synthetic inclusions of pure $H_2O$ [$T_m$ (Ice) = 0°C, $T_h$ = 374°C] and $H_2O$-$CO_2$ inclusions [$T_m$ ($CO_2$) = −56.6°C] entrapped in quartz.

Drilled calcite powder was used for stable-isotope measurements. Stable-isotope compositions of the evolved $CO_2$ gas were measured by a ThermoFinnigan delta plus XP continuous-flow mass spectrometer, using a GASBENCH II preparation device as an inlet port, at the Institute for Geochemical Research. Results are expressed using standard δ notation relative to V-PDB for C and V-SMOW for O in ‰. The reproducibility for both C and O isotope analyses is better than 0.15‰, based on replicate measurements of standards and samples.

Calculation of the oxygen isotope composition of parent fluids from the appropriate fractionation equation and the oxygen isotope composition of the mineral requires formation temperature to be very well constrained. The use of microthermometry and resulting homogenisation temperature data gives only a minimum crystallisation temperature. Increasing the temperature of a fluid with a given isotope composition would decrease the isotope composition of the precipitating calcite. And vice versa, by assuming a higher crystallisation temperature, the calculated fluid isotope composition is pushed towards less-depleted compositions. Thus, fluid isotope compositions calculated using measured homogenisation temperatures are considered here as being a minimum value of the fluids original composition.

## RESULTS

### Fluid-inclusion petrography and microthermometry

Fluid-inclusion measurements were performed on crystals of the $Cal_{EB}1$, $Dol_{ZON}$ and $Cal_{SF}$ phases. Final melting temperature data were successfully gained only in a subset of the homogenisation temperature measurements as a result of the frequent disappearance of vapour bubbles after homogenisation or freezing.

Fluid inclusions of $Cal_{EB}1$ form cloudy inclusion bands aligned along parallel growth zones in line with the scalenohedral facets of the host calcite crystals (Fig. 6A). Based on this textural feature, assemblages of these fluid inclusions are regarded as primary in origin (Goldstein & Reynolds 1994). Fluid inclusions of these primary assemblages are irregular in shape, with their longest dimension varying

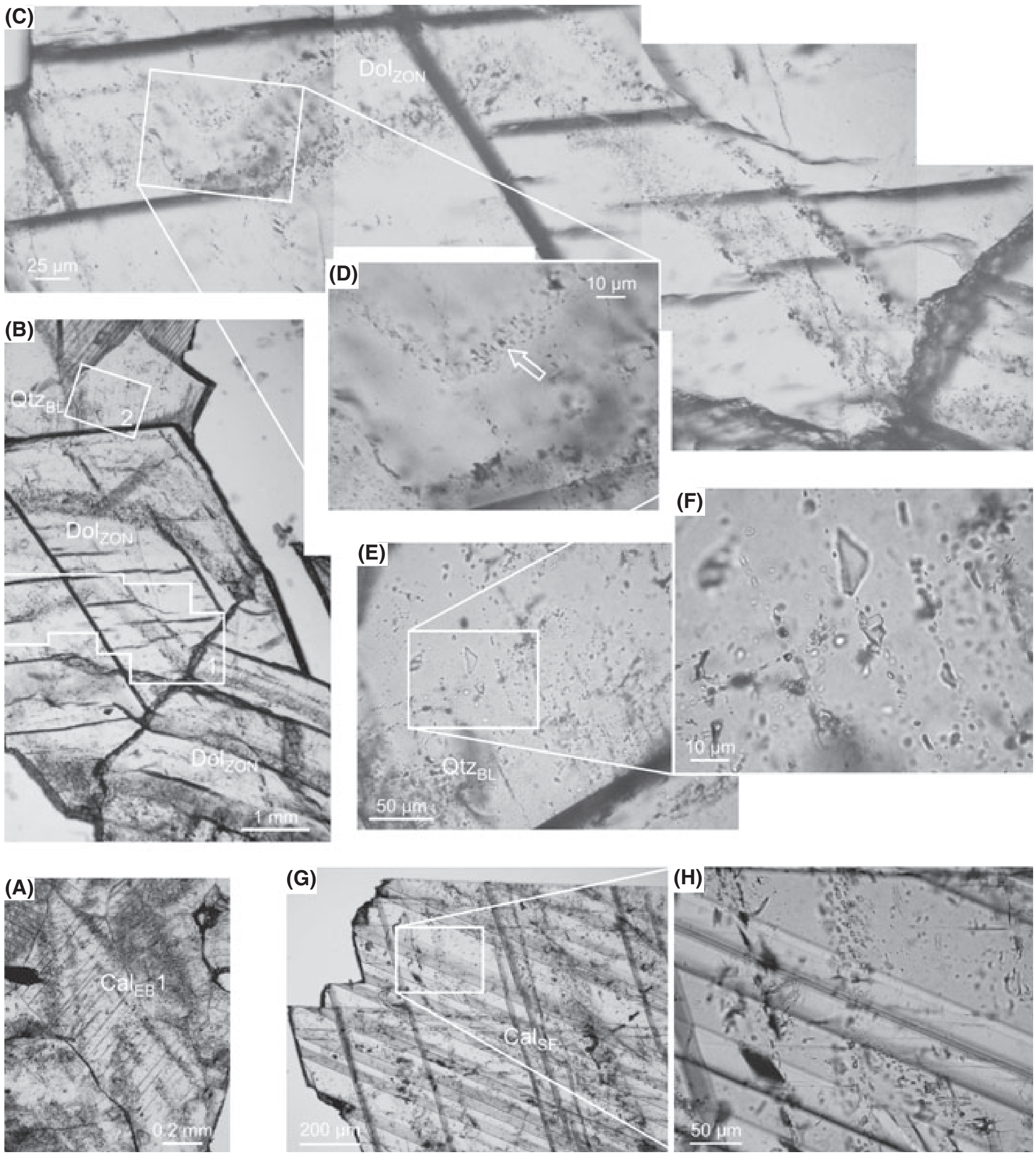


**Fig. 6.** Fluid-inclusion petrography of the vein-filling phases. (A) Primary fluid-inclusion assemblages parallel to scalenohedral facets of a $Cal_{EB}1$ crystal. (B–D) Primary fluid-inclusion assemblages parallel to rhombohedral facets of a DolZON crystal. Inset 1 in B indicates position of C, inset 2 indicates position of 6E. (E, F) Primary one-phase aqueous fluid-inclusion assemblage in a blocky quartz crystal. (G, H) Secondary inclusion trails in massive calcite ($Cal_{SF}$).

between 5 and 10 µm. Two-phase liquid-vapour aqueous inclusions occur sparsely amongst the one-phase inclusions. Fluid inclusions of differing $\varphi_V$ (25°C) value (the ratio of inclusion volume to the volume of the vapour phase in the fluid inclusion at room temperature) do not show any spatial clustering within the cloudy inclusion zones. Homogenisation temperatures of two-phase inclusions in the zone of primary inclusions are between 50 and 105°C ($n = 39$), with a maximum frequency between 75 and 90°C (Fig. 7A). Final melting temperatures are between −2.5 and −1.6°C ($n = 4$), indicating a salinity range between 2.74 and 4.2% $w$NaCl equivalent.

Zoned dolomite contains two-phase aqueous inclusions in parallel bands aligned with rhombohedral crystal facets (Fig. 6B,C). Inclusions generally display negative crystal shapes with a longest dimension of up to ~5 µm (Fig. 6D). Homogenisation temperatures range between 75 and 120°C ($n = 15$), with a maximum frequency between 95 and 100°C (Fig. 7B). Final ice-melting temperature measurements were hindered by both the lack of vapour phase nucleation after $T_h$ measurements and the loss of the vapour phase after freezing.

The blocky quartz phase ($Qtz_{BL}$) contains all-liquid aqueous inclusions (as inferred from unpublished Raman

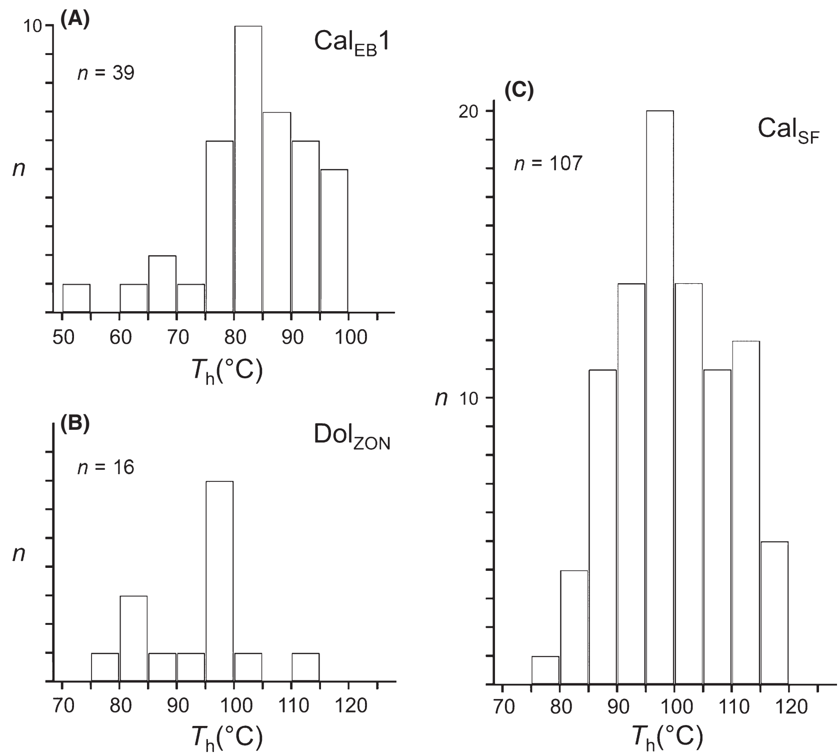


**Fig. 7.** Histograms of measured $T_h$ data in syntaxial calcite (Cal$_{EB}$1, A), zoned dolomite (Dol$_{ZON}$, B) and massive calcite (Cal$_{SF}$, C).

spectroscopy data) which are seated in irregular groups (Fig. 6E,F) and can be interpreted as primary in origin. Inclusions lengths are between 3 and 20 μm.

The massive space-filling calcite (Cal$_{SF}$) contains two-phase liquid-vapour aqueous inclusions. Sparsely occurring isolated inclusions are interpreted as primary in origin, with lengths ranging from 2 to 20 μm and generally irregular shapes. These inclusions homogenise to liquid phase between 85 and 120°C ($n$ = 92, Fig. 7C), while their final ice-melting temperatures range between −2.6 and −0.5°C ($n$ = 25, Fig. 8). Inclusions occur along trails crosscutting the massive calcite, generally having a negative crystal shape (Fig. 6G,H), and can be interpreted as secondary in origin. Secondary fluid inclusions belong to two distinct groups based on their final melting temperatures (Fig. 8). The first group has final melting temperatures between −2.1 and −1.5°C ($n$ = 7), in the range of primary inclusions, and homogenisation temperatures between 84 and 105°C, while the second group have final melting temperatures between −4.9 and −3.1°C ($n$ = 13), with similar homogenisation temperatures between 82 and 97°C.

### Carbon and oxygen isotope composition of veins

The carbon and oxygen isotope compositions of the studied veins are presented in Table 1. Graphical presentation of these results (Fig. 9A) demonstrates that samples of different texture display different isotope compositions.

Elongate blocky calcite (Cal$_{EB}$1, including data from one gneiss vein sample) displays the least depleted isotope ratios and a wide range of $\delta^{18}$O values between 23.2 and 30.3‰ and $\delta^{13}$C values between 0.3‰ and 3.3‰ (Fig. 9A). The samples analysed show a trend towards more depleted isotope values. Within-vein variations are up to 3.8‰ $\delta^{18}$O and up to 1.4‰ $\delta^{13}$C, and the data do not show any consistent relationship to distance from the vein walls. Zoned dolomite (Dol$_{ZON}$) displays $\delta^{18}$O values between 21.9‰ and 25.1‰ and $\delta^{13}$C values between −2.9‰ and −1.0‰ (Fig. 9A). The $\delta^{18}$O values of space-filling calcite (Cal$_{SF}$) range from 18.2‰ to 19.3‰, and

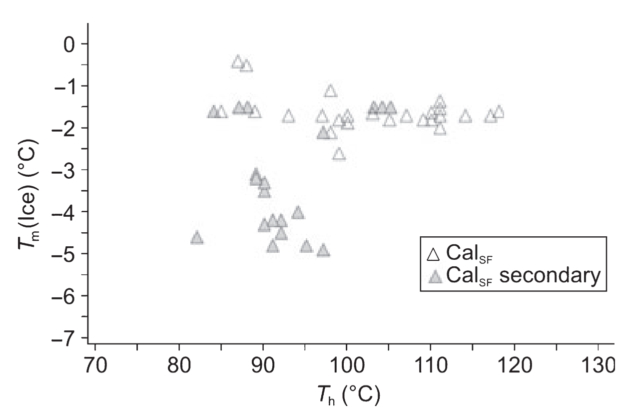


**Fig. 8.** $T_h$–$T_m$ (Ice) diagram of Cal$_{SF}$ inclusions.

$\delta^{13}C$ values from −2.3‰ to −1.9‰. Late syntaxial veins ($Cal_{EB}2$) display $\delta^{18}O$ values ranging from 20.0‰ to 21.3‰ and $\delta^{13}C$ values ranging from −10.6‰ to −9.4‰, with more depleted values in limonite-stained samples. Antitaxial veins ($Cal_{ANT}$) in gneiss display $\delta^{18}O$ values ranging from 20.6‰ to 22.7‰ and $\delta^{13}C$ values between −9.8‰ and −6.5‰, with a trend towards the less-depleted values of late syntaxial veins ($Cal_{EB}2$) in amphibolite (Fig. 9A).

## DISCUSSION

A six-stage palaeohydrological evolution model reconstructed on the basis of vein textures alone (Dabi *et al.* 2009a) is further confirmed by microthermometric and stable-isotope data. This interpretation is presented in conjunction with textural observations. Textural features, isotope compositions and minimum crystallisation temperatures of the studied vein-filling phases are summarised in Table 2.

**Table 1** Oxygen and carbon isotope compositions of studied samples.

| Sample (type) | δ13C (‰ V-PDB) | δ18O (‰ V-SMOW) |
|---|---|---|
| Amf01 ($Cal_{EB}2$) | −9.4 | 21.0 |
| Amf01 ($Cal_{EB}2$, lim.) | −9.7 | 21.3 |
| Amf02 ($Cal_{EB}1$) | 2.4 | 28.2 |
| Amf02 ($Cal_{EB}1$) | 1.8 | 26.1 |
| Amf03 ($Cal_{EB}1$) | 3.0 | 27.6 |
| Amf03 ($Cal_{EB}1$) | 2.0 | 23.8 |
| Amf03 ($Cal_{SF}$) | −1.9 | 19.3 |
| Amf03 ($Dol_{ZON}$) | −2.9 | 21.9 |
| Amf03 ($Cal_{EB}2$, lim.) | −10.6 | 20.0 |
| Amf08 ($Cal_{SF}$) | −2.3 | 18.2 |
| Amf08 ($Cal_{SF}$) | −2.1 | 18.2 |
| Amf09 ($Cal_{EB}1$) | 0.3 | 27.6 |
| Amf09 ($Cal_{EB}1$) | 2.7 | 29.6 |
| Amf10 ($Cal_{EB}1$) | 1.8 | 23.2 |
| Amf10 ($Cal_{EB}1$) | 1.1 | 25.6 |
| Amf11 ($Cal_{EB}1$) | 2.4 | 29.1 |
| Amf11 ($Cal_{EB}1$) | 2.7 | 30.1 |
| Amf11 ($Cal_{EB}1$) | 2.3 | 29.4 |
| Amf11 ($Cal_{EB}2$) | −9.5 | 21.1 |
| Amf10 ($Cal_{EB}1$) | 3.2 | 30.3 |
| AmfUNK ($Cal_{EB}2$) | −10.0 | 21.0 |
| VOL01vF ($Cal_{ANT}$) | −9.9 | 20.6 |
| VOL01vF ($Cal_{ANT}$) | −9.4 | 21.9 |
| Amf03 ($Dol_{ZON}$) | −2.7 | 22.3 |
| Amf03 ($Dol_{ZON}$) | −1.0 | 25.1 |
| VOL02vE ($Cal_{EB}1$) | 2.7 | 30.2 |
| KOV01vN ($Cal_{ANT}$) | −7.7 | 21.7 |
| KOV01vH ($Cal_{ANT}$) | −6.9 | 22.3 |
| JUH01v1 ($Cal_{ANT}$) | −7.4 | 21.9 |
| JUH01v1 ($Cal_{ANT}$) | −7.4 | 22.6 |
| JUH01v2 ($Cal_{ANT}$) | −6.5 | 22.5 |
| VOL02vB ($Cal_{ANT}$) | −9.5 | 22.7 |
| GGR01v1 ($Cal_{ANT}$) | −9.0 | 21.2 |
| GGR01vX ($Cal_{ANT}$) | −8.6 | 21.7 |

### Elongate blocky calcite ($Cal_{EB}1$)

Syntaxial elongate blocky calcite veins ($Cal_{EB}1$) are prevalent in both the amphibolite body and the outcrops of mylonitic gneiss, with distinct stable-isotope compositions suggesting similar origins. The interpretation of early occurrence in the reconstructed sequence is based on their textural relationship with subsequent carbonates: crosscutting in the amphibolite and intense twinning of syntaxial vein calcite both in the amphibolite and in the mylonitic gneiss.

Cross-cutting relations of the $Cal_{EB}1$ veins in the studied outcrop indicate at least two fluid-flow events, whereas vein textures indicate quasi continuous growth and uninterrupted fluid flow. The $Cal_{EB}1$ calcites display a range of stable-isotope compositions too wide to be interpreted as inherited from and determined by a homogenous source with which the fluid reached equilibrium. Oxygen and carbon isotope data of Cox (2007) indicate that externally derived fluids introduced into a developing fracture system may lead to variable isotopic compositions of fluids because of variable buffering by host rock, as also described by Lassey & Blattner (1988). This process can lead to significantly different isotopic compositions within spatially and temporally related veins. These deviations can be caused by variations of the reactive path length, an increase or decrease in the effective reactive surface, or variations in flow rate (Cox 2007; Barker *et al.* 2009). Thus, the wide range of oxygen and carbon isotope compositions and within-vein variations suggest that the parent fluids of the texturally uniform veins reached the site of precipitation through dynamically changing pathways. This can result from partial occlusion of the vein system because of mineral precipitation (Lee & Morse 1999; Hilgers & Urai 2002b) that diverts the fluid to pathways with different reactive lengths and thus different degrees of fluid–rock interaction (Barker *et al.* 2009). The measured differences in the isotope composition along mm-scale distances imply different fluid-flow pathways in the vein system. The wide range of measured isotopic compositions indicates that the reactive path lengths were too short for the fluids to attain isotopic equilibrium with the host rock (Barker *et al.* 2009). Isotope data from transecting veins may be more representative of the unbuffered parent fluid because, according to the model of Lassey & Blattner (1988), the fluid–rock system becomes more fluid-buffered during its evolution, so the late veins of a vein generation are less rock-buffered. The $\delta^{18}O$ and $\delta^{13}C$ values of late $Cal_{EB}1$ veins are the highest amongst the samples, suggesting that the heaviest isotope compositions reflect equilibrium with the least rock-buffered fluids.

The presence of one-phase fluid inclusions in primary assemblages of $Cal_{EB}1$ suggests low-temperature precipitation (<50°C, Goldstein & Reynolds 1994). The measured

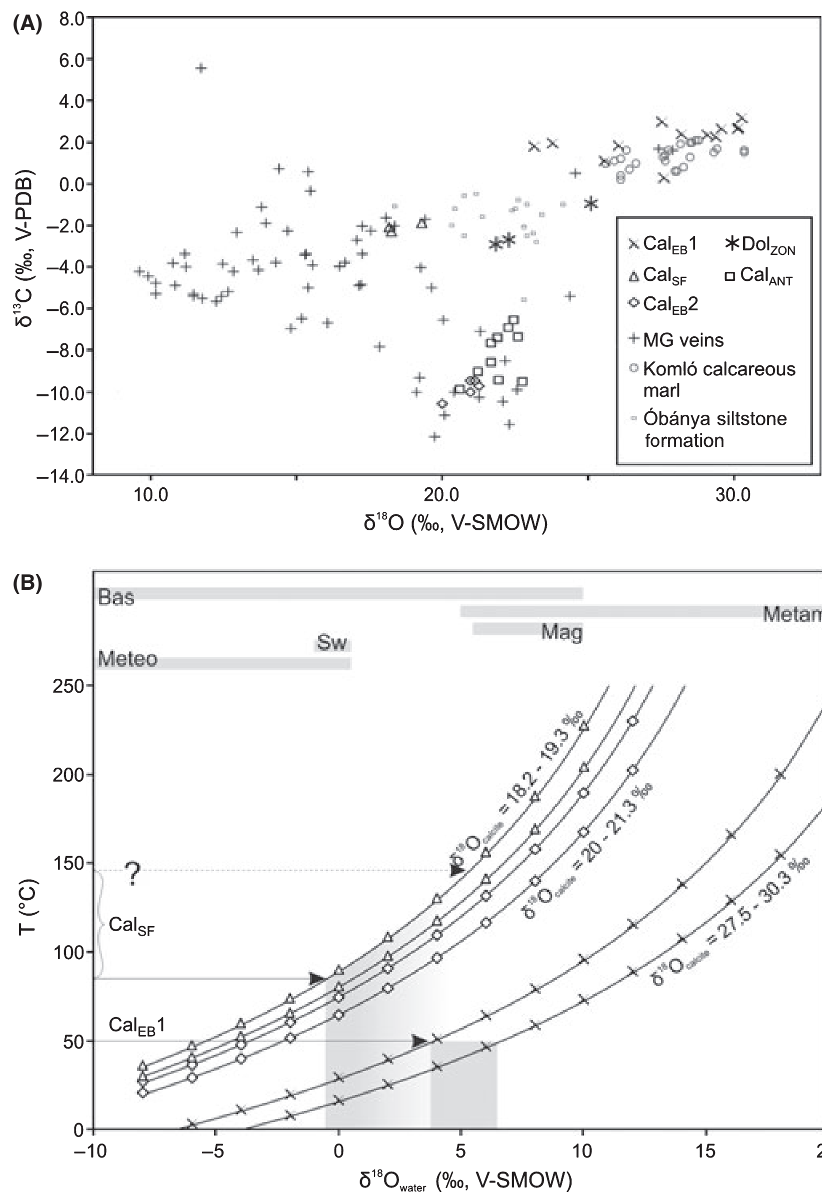


**Fig. 9.** (A) Stable-isotope compositions of vein calcites. Vein isotope compositions of the Mórágy Granite Formation to the south (MG veins, Kovács-Pálffy & Földvári 2003), the Komló Calcareous Marl Formation (Raucsik 1997) and the Óbánya Siltstone Formation (Varga *et al.* 2007) are also indicated. (B) Temperature-$\delta^{18}O_{water}$ plot of vein calcites. The curved lines represent $\delta^{18}O$ values of samples of different textural types. Knowledge of the formation temperature permits the calculation of the oxygen isotope composition of the parent fluid (horizontal axis) using the relevant fractionation equations. The isotopic range of fluids of different origin is also indicated (Taylor 1987): Meteo., meteoric water; Bas., basinal brine; Sw., seawater; Mag., magmatic; Metam., metamorphic.

**Table 2** Features of the successive vein-filling phases. Crystallisation temperatures are minima, as suggested by the lowest measured homogenisation temperature of the fluid inclusions that contain the parent fluid.

| | Host rock/texture | | | Isotope composition | | |
|---|---|---|---|---|---|---|
| | Amphibolite | Gneiss | Cathodoluminescence | ‰ (SMOW) | ‰ (PDB) | Crystallisation temperature |
| $Cal_{EB}1$ | Syntaxial | Syntaxial | Brecciated, metasomatised | 23.2 to 30.3 | 0.3 to 3.3 | Max. 50°C |
| $Dol_{ZON}$ | Syntaxial | | Red, oscillatory | 21.9 to 25.1 | −2.9 to −1.0 | Min. 75°C |
| $Qtz_{BL}$ | Syntaxial | | | | | Max. 50°C |
| $Cal_{SF}$ | Massive | | Orange | 18.2 to 19.3 | −2.3 to −1.9 | Min. 85°C |
| $Cal_{MASS}$ | Massive | | Dull | | | Min. 82°C |
| $Cal_{EB}2$ | Syntaxial | | Dull (limonite stained) | 20.0 to 21.3 | −10.6 to −9.4 | 240(?)°C |
| $Cal_{ANT}$ | | Antitaxial | | 20.6 to 22.7 | −9.9 to −6.5 | |

two-phase inclusions are interpreted to be primary inclusions stretched during subsequent thermal evolution of the MZ, because they do not show any spatial clustering within the cloudy inclusion zones. Thus, the measured homogenisation temperatures of these inclusions do not apply to the temperature of crystallisation, but their final melting temperatures are valid for the salinity of the parent fluid (between 2.74 and 4.2% *w*NaCl equivalent). Applying a crystallisation temperature of 50°C and using the fractionation equation of O'Neil *et al.* (1969), the calculated oxygen isotope composition of the parent fluid is between 3.8‰ and 6.6‰ (Fig. 9B). This value suggests a fluid of basinal, metamorphic or magmatic origin (Taylor 1987; Blyth *et al.* 2000), or a fluid exchanged with rock. Liquid aqueous inclusions imply crystallisation temperatures near or below 50°C (Goldstein & Reynolds 1994), which casts doubt upon a magmatic or metamorphic origin. If the fluid is of metamorphic or magmatic origin, a temperature drop is implied, which is inconsistent with calcite precipitation, because the decrease in fluid temperature at constant salinity increases calcite solubility, and vice versa (Parry 1998). Isothermal precipitation is possible during decompression of fluid that is saturated with dissolved carbon dioxide (Parry 1998). Such a process might occur if a rock-fracturing event were to open new porosity, lower fluid pressure and cause effervescence of dissolved $CO_2$. The similarity of the isotopic composition of $Cal_{EB}1$ calcite to Mesozoic carbonaceous formations to the north, and to marine carbonates in general (Prokoph *et al.* 2008), may provide a possible clue as to the fluid source. According to the best knowledge of the authors, stable-isotope data have been published only from the Toarcian Óbánya Siltstone Formation (Varga *et al.* 2007) and the Toarcian – Bajocian Komló Calcareous Marl Formation (Raucsik 1997; Fig. 9A). The similarity between the vein isotopic compositions and the latter data suggests that the parent fluid is related to Mesozoic carbonaceous sediments. If so, because deposition of carbonaceous sediments began during the Middle Triassic (Anisian Lapisi Limestone Formation), the $Cal_{EB}1$ fluid-flow event could not have occurred before the Anisian.

A syntaxial elongate blocky texture is indicative of advective fluid transport through a fracture system that tends to clogg, as demonstrated by the experimental studies of Hilgers & Urai (2002b) and Hilgers *et al.* (2003). This process produces partially filled fracture systems, with decreasing filling with distance from the obstruction, because of a shift in saturation state along the flow pathway. Lee *et al.* (1996) and Lee & Morse (1999) pointed out that fairly uniform deposition of calcite can occur only if the flow is quite rapid (tens to thousands of cm $h^{-1}$), because of the risk of high supersaturation. (G. Dabi, T. M. Tóth & F. Schubert, unpublished conference abstract, 2006) described oscillatory zoning in grains of $Cal_{EB}1$. The presence of latent oscillation along lines subparallel to the growth directions indicates surface enrichment during mineral growth and that the growth rate of the crystal was greater than the diffusion rate of the trace element in the surface layer at the temperature of crystallisation (Watson 1996, 2004). (G. Dabi, T. M. Tóth & F. Schubert, unpublished conference abstract, 2006) detected the oscillatory zoning with UV luminescent microscopy, so the trace element responsible for the oscillation is not known. The lack of data on the diffusion rate of the oscillatory trace element hampers conclusions on crystal growth rates and saturation.

### Zoned dolomite ($Dol_{ZON}$)

Red luminescent patches on the $Cal_{EB}1$ cathodoluminescence images suggest that the parent fluid of $Dol_{ZON}$ percolated through grains of $Cal_{EB}1$, at least locally within the amphibolite body. Dolomite veins were not found by the authors, although it is possible that they exist, according to unpublished field reports (S. Józsa, Eötvös University, oral communication, 2007). Crystallisation of the zoned dolomite occurred in closed remnant voids, as suggested by the lack of dolomite veins cutting through crystals of $Cal_{EB}1$. Applying a crystallisation temperature of 95°C (the minimum crystallisation temperature according to the distribution of the measured $T_h$ data, Fig. 7A) and using Northrop & Clayton's (1966) fractionation equation for dolomite (in Friedman & O'Neil 1977), the minimum oxygen isotope composition of the parent fluid is between −0.2‰ and 3.0‰, indicative of a basinal brine, seawater or meteoric water (Taylor 1987).

### Blocky quartz ($Qtz_{BL}$)

Primary, all-liquid fluid inclusions in the blocky quartz $Qtz_{BL}$ suggest low-temperature entrapment of fluids and crystallisation. All-liquid fluid inclusions are indicative of low-temperature fluids (below 50°C, Goldstein & Reynolds 1994) and possible meteoric origin. The syntaxial texture and the presence of thin veins transecting preceding phases suggest fracture-channelised flow of the parent fluid.

### Space-filling calcite ($Cal_{SF}$)

Massive space-filling calcite was found only in the remnant voids of veins crosscutting the amphibolite body. The orange luminescent colour of both the $Cal_{SF}$ calcite and the swarms of microveins cutting through earlier $Cal_{EB}1$ and $Dol_{ZON}$ suggests that the fluid-flow event that produced $Cal_{SF}$ included brecciation of the pre-existing vein system. Homogenisation temperatures of the primary, two-phase fluid inclusions range from 85 to 119°C, with last melting temperatures between −2.6 and −0.4°C (salinities between 0.7 and 4.7% *w*NaCl equivalent). The presence of secondary fluid inclusions with the same range of last melting temperatures [$T_m$ (Ice) between −2.1 and −1.5°C and salinities between 2.57 and 3.55% *w*NaCl equivalent] but lower homogenisation temperatures ($T_h$ between 85 and 105°C) implies that the $Cal_{SF}$ parent fluid was present during failure of the vein system (as revealed by the brecciated vein segments) and experienced intermittent flow. Dabi *et al.* (2009a) found veins of similar orange CL colour displaying ataxial crack-seal texture. The identification of these veins as space-filling calcite further confirms the intermittent flow of the $Cal_{SF}$ parent fluid. Differences in the $T_h$ data can be interpreted as representing differences in fluid density, with higher homogenisation temperatures equivalent to lower fluid density and vice versa. Assuming that the space-filling calcite was precipitated from the same fluid as that in the secondary inclusions, the first failure event permitted a greater pressure drop and thus greater density drop of the fluid because of the availability of remnant voids. Subsequent failure events permitted only smaller pressure drops and thus higher densities, reflected by the distinctly lower $T_h$ range of the secondary inclusions.

Szabó *et al.* (2008) and Poros *et al.* (2008) detected a regional fluid-flow event with fluid salinity in the same range as the primary fluids in $Cal_{SF}$. This fluid was also detected in FIPs of rock-forming quartz in the Mórágy Granite Formation to the south. Fourcade *et al.* (2002) interpreted disseminated carbonates in whole rock samples as being precipitated from fluids that once pervaded the rock matrix. The possible match between the orange luminescent calcite seams of rock-forming minerals in mylonitic gneiss (Fig. 5A) and space-filling calcite potentially confirms percolation of the $Cal_{SF}$ parent fluid and its volatile origin related to the Early Cretaceous dyke emplacement.

Stable-isotope composition of $Cal_{SF}$ calcite is between 18.2‰ and 19.3‰ for oxygen and between −2.3‰ and −1.9‰ for carbon. Assuming a crystallisation temperature of 85°C – consistent with the lowest homogenisation temperature of the primary inclusions – the $\delta^{18}O_{fluid}$ value is between −0.6‰ and 0.5‰, indicative of meteoric water, basinal brine or seawater (Fig. 9B). However, failure caused by fluid is more likely at higher fluid pressures. A higher fluid and crystallisation temperature is possible and a certain amount of pressure correction can be applied. For example, applying a higher crystallisation temperature of 140°C – consistent with a fluid pressure of ca. 80 MPa – would result in a $\delta^{18}O_{fluid}$ value of between 4.8‰ and 5.9‰, indicative of basinal brine or magmatic and metamorphic water (Taylor 1987).

### Red massive calcite ($Cal_{MASS}$)

The red calcite contained solid inclusions of quartz and spherulitic haematite and lacked fluid inclusions. Because the preceding $Cal_{SF}$ calcite contained two secondary fluid generations (one of which represents the $Cal_{SF}$ parent fluid), and $Cal_{EB}2$ was subsequently precipitated from a fluid of different salinity (Dabi *et al.* 2009b), it is plausible that the secondary inclusions of $Cal_{SF}$, with their lower final melting temperatures (Fig. 8), could have trapped the parent fluid of $Cal_{MASS}$. The fluid entrapped in the higher salinity secondary inclusions of $Cal_{SF}$ [$T_h$ between 82 and 97°C and $T_m$ (Ice) between −4.8 and −3.1°C, corresponding to salinities between 5.1 and 7.6% *w*NaCl equivalent] may be the parent fluid of $Cal_{MASS}$.

A number of experimental investigations regarding the formation of spherulitic haematites have been carried out (Kandori *et al.* 2000, 2002), but few if any have modelled fluids that are analogues of real crustal fluids. The cross-cutting relationship of the veins demonstrates that the red massive calcite-producing flow event preceded $Cal_{EB}2$ and $Cal_{ANT}$, and thus also the pre-Gosau tectonic movements of the Early to Late Cretaceous (see below). The pre-Gosau tectonic movements were preceded by basanitic to phonolitic volcanism between 135 and 110 Ma (Harangi 1994). Analogies with the Mauna Kea hydrothermal spherulitic haematites (Morris *et al.* 2005) and the presence of both alkaline basalt and alkaline trachyte dykes related to the Early Cretaceous Eastern Mecsek basaltic volcanism (Balla *et al.* 2009) suggest the potential role of volcanic activity in producing the red massive calcite.

### Late syntaxial and antitaxial veins

In the Mórágy granite to the south, Koroknai (in Balla *et al.* 2009) noted that 'thinner dykes locally continue upwards in fractures filled with carbonate and limonitic material, from which the rock material of the dyke has partly or completely vanished'. Thus, it can reasonably be assumed that the limonite-stained calcites are related to Cretaceous dyke emplacement and volatile escape. This assumption is further constrained by the similarity of the $Cal_{ANT}$ parent fluids (Dabi *et al.* 2009b) to the fluids of the regional fluid-flow events defined by Szabó *et al.* (2008) and Poros *et al.* (2008).

Late syntaxial calcite ($Cal_{EB}2$) within the amphibolite body contains no fluid inclusions. The orange limonite-stained zone at the vein-wall interface of these veins suggests that precipitation of orange calcite preceded white calcite. The presence of limonite-stained calcite in antitaxial veins indicates a possible common parent fluid for $Cal_{EB}2$ and $Cal_{ANT}$. This suggestion is reinforced by their shared order of precipitation, as inferred from texture and the lack of calcite twins in both late syntaxial and antitaxial veins. Trails and bands of solid inclusions record a crack-seal process during vein growth (Ramsay 1980; Hilgers & Urai 2005), which in turn is interpreted as the result of fluid pressure fluctuations by Etheridge *et al.* (1984) and Bons (2000). Although interpretation of homogenisation temperature measurements in calcite is difficult, especially if trapping of fluids occurs during fluid-pressure fluctuation, previous microthermometric studies of Dabi *et al.* (2009b) on primary inclusions of the antitaxial veins imply supralithostatic fluid pressures during vein growth. Curvature of grain boundaries suggests that sequential growth of the antitaxial veins proceeded through a sequence of extensional shear mode openings (Bons 2001; Hilgers *et al.* 2001). According to the model of Sibson (1998), supralithostatic fluid pressures can lead to extensional shear only in a compressional tectonic regime (see Fig. 2 in Sibson 1998).

Salinity of antitaxial calcite parent fluids is between 0.18 and 0.53 *w*NaCl equivalent (Dabi *et al.* 2009b). The range of salinities of the regional flow event defined by Szabó *et al.* (2008) and Poros *et al.* (2008) in the Mórágy Granite to the south overlaps with the salinities measured in primary inclusions of space-filling calcite ($Cal_{SF}$) and antitaxial calcite ($Cal_{ANT}$). Both authors detected the flow event in healed microcracks within rock-forming quartz so, assuming that these fluids are the same as the parent fluids of massive space-filling ($Cal_{SF}$) and antitaxial ($Cal_{ANT}$) calcite, it is plausible that the parent fluids of both $Cal_{SF}$ and $Cal_{ANT}$ pervaded the rock matrix. An antitaxial texture is in itself indicative of percolation of parent fluids through host rock, according to Bons (2000), Hilgers & Urai (2002a) and Hilgers & Sindern (2005). Furthermore, the stable-isotope data from antitaxial veins display a trend towards the more depleted compositions of their syntaxial counterparts (Fig. 9A). Such a trend is similar to the distribution of stable-isotope data from antitaxial and syntaxial veins produced by the same fluid in limestone, as described by Rye & Bradbury (1988), who interpreted the data from antitaxial veins as reflecting different degrees of buffering by the host rock during flow along the developing stylolite system. The narrower range of syntaxial veins was considered to be in isotope equilibrium with the parent fluid. Based on all the aforementioned considerations, herewith we regard the fluid flow of $Cal_{ANT}$ parent fluids as being pervasive through the host rock. Furthermore, based on textural observations, late syntaxial calcite veins evolved in the amphibolite bodies contemporaneously with antitaxial veins in the gneissic host. Thus, the presence of syntaxial veins in the amphibolite bodies suggests that the fracture system in the amphibolite bodies acted as rapid fluid conduits connected to the fluid source. At the same time antitaxial counterparts in the gneissic host, and the trend of their isotope compositions towards more rock-buffered values, indicate pervasive flow of the same parent fluid.

#### Palaeohydrological evolution and interactions of the Mecsekalja Zone

The combination of stable-isotope and microthermometric data suggests a two-stage evolution of the sheared crystalline rocks of the Ófalu Formation, consistent with the Mesozoic subsidence history of the study area as reconstructed by Császár (2003, Fig. 10).

The first stage is characterised by fluids of carbonaceous, possibly Mesozoic affinity, and low-temperature fluids presumably derived from carbonaceous sediments ($Cal_{EB}1$), basinal brines ($Dol_{ZON}$) and meteoric fluids ($Qtz_{BL}$). This sequence is consistent with a shallow crustal position of the MZ (trapping temperatures below 50°C), although $Dol_{ZON}$ represents a deeper parent fluid (minimum trapping temperature of 75–100°C) and perhaps a short subsidence period. The $Cal_{EB}1$ parent fluid equilibrated with Mesozoic carbonaceous rocks, and the deposition of carbonaceous sediments in the region began in the Anisian (Török 1998), so the earliest time for potential $Cal_{EB}1$ precipitation is Middle Triassic (Fig. 10). A shallow crustal position of the southern foreland is suggested during the Pliensbachian (Némedi Varga 1998), whereas heavy-mineral studies of Toarcian black shale (Varga *et al.* 2009) in the Mecsek Mountains suggest denudation of metamorphic rocks. Thus, geological evidence is also suggestive of a shallow crustal position for the low-temperature meteoric fluid-flow event that produced the blocky quartz (Fig. 10). Assuming a possible basinal origin of the fluids and their higher temperature in comparison with the $Cal_{EB}1$ fluids, precipitation of $Dol_{ZON}$ most likely occurred between the early Upper Triassic and the Middle Liassic, when the sedimentary sequences were thickest. Comparison of isotope data from these early carbonate phases with stable-isotope

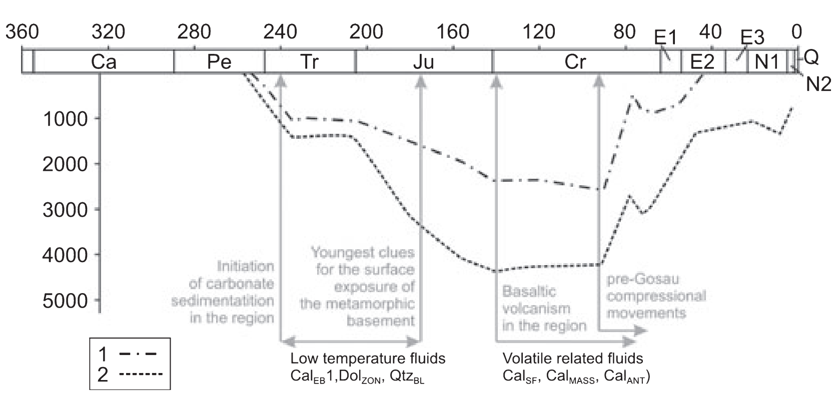


**Fig. 10.** Subsidence curves of the Mórágy Block, including the MZ (1) and the Zsibrik Block to the north (2) in the Mesozoic, after Császár (2003). Horizontal arrows mark the time intervals of formations of the vein-filling phases, vertical arrows mark different geologic events that delineate the time of vein formation. See text for details.

data from the Mórágy Granite (Fig. 9A) suggests that the fluid evolution of the two complexes was not linked during the Triassic to Late Jurassic.

The second stage ($Cal_{SF}$, $Cal_{MASS}$, $Cal_{EB}2$ and $Cal_{ANT}$) is characterised by low-salinity fluids possibly pervaded through the rock matrix. The similarity of these fluids to those defined by Poros *et al.* (2008) and Szabó *et al.* (2008) suggests that the MZ and the Mórágy Granite complex became part of the same hydraulic system. The second stage is also consistent with subsidence of the rocks to a maximum burial depth between 4000 and 5000 m (Császár 2003). A relation between these fluids and the Cretaceous volcanic activity and dyke emplacement is suggested by the pervasive carbonatisation ($Cal_{SF}$), coprecipitation with spherulitic haematite ($Cal_{MASS}$) and the limonite-stained calcites ($Cal_{EB}2$, $Cal_{ANT}$), especially if we consider their direct association with the dykes, as described by Koroknai (in Balla *et al.* 2009). Initiation of the volcanism in the Late Berriasian–Early Valanginian constrains the earliest time of $Cal_{SF}$ deposition (Fig. 10).

The temperature history defined by the succession of vein minerals corresponds to the Triassic to Late Cretaceous evolution of the region. Based on the sedimentary sequences of the Mecsek Mountains, transgression began in the Anisian and lasted until the Carnian. Based on the relationship of $Cal_{EB}1$ calcite to Triassic and Jurassic carbonaceous formations, the Anisian is also the earliest starting date for the fluid-flow event/precipitation. From the end of the early Middle Triassic until the Middle Liassic, thick successions of fluvial and lagoon sediments were deposited. In the Middle Liassic, subsidence of the region began and deposition of shallow marine to pelagic marls occurred. A shallow crustal position of the southern foreland is suggested during the Pliensbachian (Némedi Varga 1998), and heavy-mineral studies of Toarcian black shale (Varga *et al.* 2009) in the Mecsek Mountains suggest denudation of the underlying metamorphic rocks. This geological evidence suggests a shallow crustal position for the low-temperature meteoric fluid-flow event that produced the blocky quartz ($Qtz_{BL}$). Based on a possible basinal origin of the fluids and their higher temperature relative to the $Cal_{EB}1$ fluids, precipitation of $Dol_{ZON}$ most likely occurred between early Upper Triassic and the Middle Liassic, when the sedimentary sequences were thickest. According to the subsidence curve of Császár (2003), a similarly shallow Triassic burial depth can be inferred for the crystalline-cover interface of both the Mórágy Block (including the MSZ) and the Zsibrik Block to the north. For the Jurassic and Cretaceous, faster and deeper subsidence of the Zsibrik Block was calculated, with a maximum burial depth of ca. 4400 m between the Late Jurassic and the Late Cretaceous. For the Mórágy Block, a maximum burial depth of ca. 2400 m was assumed for the same time interval. Uplift of both blocks began during the pre-Gosau orogenic phase in the Turonian. The denudation of the crystalline rocks of the Mórágy Block commenced during the Middle Eocene, and the crystalline basement of the carbonaceous rocks has not reached the surface (Császár 2003).

### Implications of vein texture for the hydraulic behaviour of a heterogeneous rock mass

In the second stage of the palaeohydraulic evolution of the MZ, volatiles related to the Early Cretaceous dyke emplacement governed the hydrogeology of the MZ metamorphic complex. The parent fluids of both $Cal_{SF}$ and $Cal_{ANT}$ percolated through the host rock. The differences between these phases – the possible relation between pervasive carbonatisation and $Cal_{SF}$, and the development of antitaxial veins related to the flow of the $Cal_{ANT}$ parent fluid – motivate a two-stage, stress-dependent hydraulic model.

The early stage records pervasion of volcanic fluids in an extensional regime. Dyke emplacement itself typically indicates an extensional tectonic regime, with the trend of the newly opened dykes parallel to the horizontal $\sigma_2$ axis and perpendicular to the $\sigma_3$ axis (also horizontal: Best 2003). In the MZ, volatile-related fluids ruptured the rock along individual grain boundaries and deposited calcite films (Fig. 11A), similar to the Mórágy Granite to the south (Balla *et al.* 2009). In the later stage, the regional stress field became compressional (Early Albian, Fig. 10) but, according to cross-cutting relations between dykes and folded structures in the Mecsek Mountains, dyke emplacement did not cease. The volatile origin of the limonite-stained carbonates (Balla *et al.* 2009) and the formation of the $Cal_{ANT}$ veins in a compressional regime, as implied by vein textures and fluid-inclusion microthermometry (Dabi *et al.* 2009b), suggest that the deposition of the limonite-stained calcites occured in the second, compressional stage (Fig. 11B).

The deposition of limonite-stained calcites with basically different textures in the amphibolite (syntaxial $Cal_{EB}2$) and in the gneissic host (antitaxial, $Cal_{ANT}$, Fig. 11C,D) calls for a rock-dependent hydraulic model in the compressional stage. Rock-dependent hydraulic behaviour is also indicated by the different extent of buffering of the parent fluids, as implied by different ranges of isotope compositions for the two textural types (Fig. 9A).

Crack-seal textures in antitaxial veins suggest subsequent fluid batches in a sequentially dilating vein or vein system (Bons 2000; Hilgers & Urai 2005). The extent of the individual opening increments is on the order of tens of microns in the studied veins (as implied by distance between solid inclusion bands). Syntaxial counterparts in the amphibolite bodies indicate quasi-continuous single-flow events, where the apertures of the single fractures are on the order of thousands of microns. This difference in aperture of the singular-flow pathways is consistent with

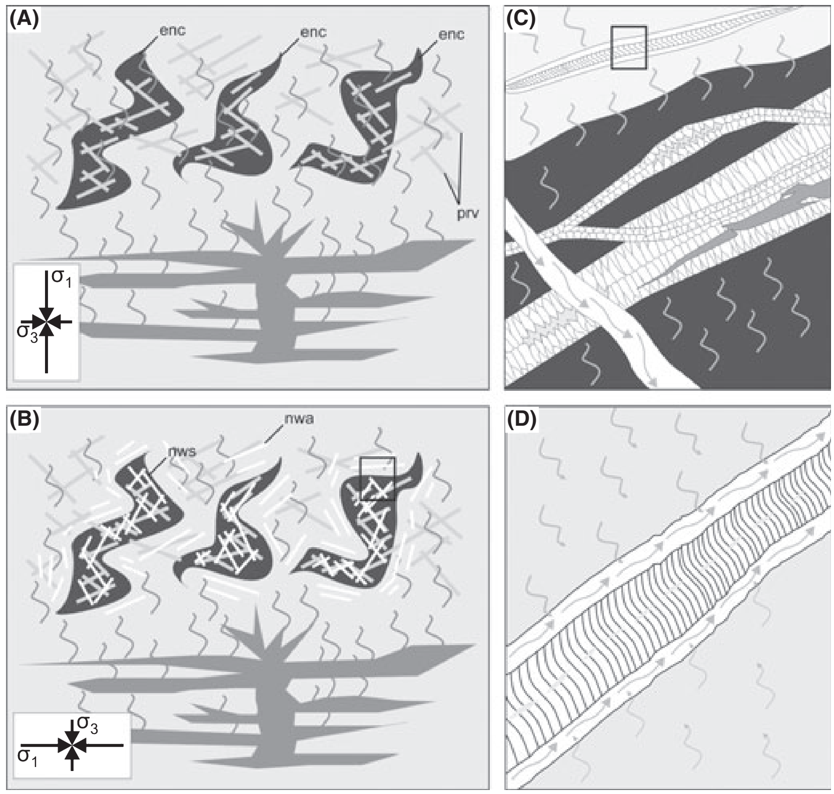


**Fig. 11.** Process diagram of dyke emplacement-related flow events. (A) Escape during decompression and pervasion of fluids during the first stage of the Cretaceous volcanic activity in an extensional stress regime. Calcite deposition occurred in remnant voids of the pre-existing vein system and along grain boundaries in the host rocks, forming thin films around the single grains. Wavy lines in the host rock symbolise pervasion of fluids. (B) In the second stage, pervasion of fluids continued, but the tectonic regime became compressional. The limonite-stained calcite parent fluids flowed advectively in several-mm-wide fractures in the amphibolites enclaves, and percolated through the host rocks. Antitaxial veins opened parallel to foliation in the mylonite gneiss and were sites of deposition. The two fracture system did not communicate. enc, amphibolites enclave; prv, pre-existing veins (grey stripes); nwa, newly opened antitaxial veins; nws, newly opened syntaxial veins (white stripes). Inset indicates the position of C. (C) Fracture in the amphibolite (dark grey) is several mm wide and acts as a rapid fluid-flow conduit (fracture-channelised flow). The simultaneously opening increment in the antitaxial vein crosscutting the gneissic host (light grey) is only about ten micron. Inset indicates the position of D. Not to scale. (D) Opening increment of the antitaxial vein occurs along the interface between the pre-existing vein and the gneissic host (antitaxial growth). Percolating fluids invade the newly opened volumes along the vein-host interface (Hilgers & Urai 2002a), and fracture-channelised flow occurs in the newly opened space between the pre-existing vein and the host. Grain boundaries of the pre-existing vein are curved, indicating the opening directions during vein growth (Bons 2000). Not to scale.

much longer flow distances, assuming a similar level of calcite saturation for both parent fluids (Lee *et al.* 1996; Lee & Morse 1999). The smaller range of stable-isotope compositions in syntaxial veins, compared to antitaxial veins, implies that fluids of the same origin were not connected in the two rock types. Hilgers & Urai (2002a) described antitaxial en echelon veins; their observations imply that the parent fluids entered the site of precipitation along the pre-existing vein-host interface. The veins that they studied were isolated in three dimensions. Although the entire lengths of the MZ antitaxial veins could not be observed due poor outcrop exposure, their maximum thickness is ca. 5 mm. Thus, assuming a lens-like shape, their insularity is likely, at least in places where they do not occur in vein systems. The wide range of isotopic compositions implies a high degree of rock-buffering of the antitaxial parent fluids, while the narrow range in syntaxial veins is interpreted to be inherited from the source (Rye & Bradbury 1988). If the coexisting fluids of the two subsystems were connected, then a similar range of isotope compositions should be expected to evolve as a result of mixing. Thus, we assume that the amphibolite bodies acted as rapid long-distance flow systems with a small degree of fluid buffering and direct connection to the source. At the same time, the vein system of the surrounding gneissic rocks contained batches of fluids from the same source, but with varying lengths of pervasion through the host rock (compare Fig. 11C,D). The two vein systems were not connected during vein development. Similar compartmentalised fluid flow is described in the Szeghalom Dome, in the north-eastern part of the TMU (M. Tóth *et al.* 2004; Schubert *et al.* 2007), where vein minerals shed light on the distinct fracture systems of gneissic rocks and embedded amphibolite bodies.

Similar hydraulic behaviour has been described from limestones in a Pyrenean thrust ramp, although there the antitaxial veins preceded the syntaxial veins (Rye & Bradbury 1988). Both in the Pyrenean thrust and in the MZ, antitaxial veins are assumed to form in an active compressional tectonic regime. In the Pyrenean limestones, the fluid flow appears to be concentrated along contemporaneous syntectonic stylolites. In case of the MZ crystalline rocks, active compression presumably led to extensive pervasion of the parent fluids by keeping microfractures open (Lespinasse 1999). The lack of antitaxial veins in the studied amphibolite bodies may result from its brittle behaviour versus the more ductile behaviour of the mylonitic gneiss. The present results raise the possibility that the formation of antitaxial veins suggests a compressional regime.

## CONCLUSIONS

A two-stage palaeohydrological evolution has been reconstructed for the Mecsekalja Zone, the first of which is characterised by fluids possibly related to marine carbonaceous formations, basinal brines and meteoric waters. This stage is consistent with the shallow crustal position of the MZ until the Early Jurassic. In the second stage, the rock mass was intruded by fluids related to the Cretaceous volcanism, as implied by compatibility between the $Cal_{SF}$ calcite and pervasive, volatile-related fluids, and the direct connection between dykes and limonitic carbonates ($Cal_{EB}2$, $Cal_{ANT}$). This second stage was synchronous with the Middle Jurassic to Late Cretaceous subsidence. Similarity between the second-stage parent fluids and fluids entrapped in FIPs of rock-forming quartz in the granite to the south suggests pervasive fluids in the second stage. Cathodoluminescence microscopy analysis revealed brecciation of earlier carbonates and possible hydrofracturing because of over-pressurisation during the production of massive calcite ($Cal_{SF}$). The possibility of episodic overpressure is supported by the similar chemistry but differing densities of primary and secondary fluids as suggested by microthermometry. Antitaxial crack-seal textures and curved grain boundaries of the youngest vein generation suggest a compressional tectonic regime, possibly related to the pre-Gosau tectonic movements in the Late Cretaceous. The stable-isotope compositions imply pervasive flow of parent fluids through the host rock of the antitaxial veins. Stable-isotope compositions of the same vein generation (including syntaxial counterparts in the amphibolites) imply distinct action of the two contemporarily developing vein systems and differing hydraulic behaviour of the mylonitic gneiss and the amphibolite bodies.

## ACKNOWLEDGEMENTS

This project was financially supported by the OTKA Foundation (Grant No. K60768). We thank Shaun L.L. Barker, Steve Ingebritsen and an anonymous reviewer whose comments and recommendations have highly improved the manuscript.

## REFERENCES

Árkai P, Nagy G (1994) Tectonic and magmatic effects on amphibole chemistry in mylonitized amphibolites and amphibole bearing enclaves associated with granitoid rocks. *Acta Geologica Hungarica*, **37**, 235–68.

Balla Gy, Császár G, Gulácsi Z, Gyalog L, Kaiser M, Király E, Koloszár L, Koroknai B, Magyari Á, Maros Gy, Marsi I, Molnár P, Rotárné Szalkai Á, Tóth G (2009) *Geology of the North-eastern Part of the Mórágy Block. Regional Map-series of Hungary*, pp. 73–81. Geological Institute of Hungary, Budapest.

Barker SLL, Cox SF, Eggins SM, Gagan MK (2006) Microchemical evidence for episodic growth of antitaxial veins during fracture-controlled fluid flow. *Earth and Planetary Science Letters*, **250**, 331–44.

Barker SLL, Bennett VC, Cox SF, Norman MD, Gagan MK (2009) Sm-Nd, Sr, C and O isotope systematics in hydrothermal calcite-fluorite veins: implications for fluid-rock reaction and geochronology. *Chemical Geology*, **268**, 58–66.

Best MG (2003) *Igneous and Metamorphic Petrology*, 2nd edn. Blackwell Publishing.

Blyth A, Frape S, Blomqvist R, Nissinen P (2000) Assessing the past thermal and chemical history of fluids in crystalline rock by combining fluid inclusion and isotopic investigations of fracture calcite. *Applied Geochemistry*, **15**, 1417–37.

Bodnar RJ (1992) Revised equation and table for freezing point depressions of $H_2O$-salt fluid inclusions. *PACROFI IV, Fourth Biennial Pan-American Conference on Research on Fluid Inclusions, Lake Arrowhead, Abstract*, pp. 108–11.

Bons PD (2000) The formation of veins and their microstructures. In: *Stress, Strain and Structure, A Volume in Honour of W.D Means* (eds Jessel MW, Urai JL) *Journal of the Virtual Explorer*, **32**, 2.

Bons PD (2001) Development of crystal morphology during unitaxial growth in a progressively widening vein: I. The numerical model. *Journal of Structural Geology*, **23**, 865–72.

Bottomley JD, Veizer J (1992) The nature of groundwater flow in fractured rock: evidence from the chemical and isotopic evolution of recrystallized fracture calcites from the Canadian Precambrian Shield. *Geochimica et Cosmochimica Acta*, **56**, 369–88.

Cox SF (2007) Structural and isotopic constraints on fluid flow regimes and fluid pathways during upper crustal deformation: an example from the Taemas area of the Lachlan Orogen, SE Australia. *Journal of Geophysical Research*, **112**, B08208, doi: 10.1029/2006JB004734.

Császár G (2003) Alpine burial history of the Mórágy Block and its environs. In: *Annual Report of the Geological Institute of Hungary 2003* (ed. Balla Z), pp. 395–406.

Császár G, Görög Á, Gyuricza Gy, Sieglné Farkas Á, Szente I, Szinger B (2007) The geological, paleontological and sedimentological pattern of the Vasas Marl Formation between Zsibrik and Ófalu, South Transdanubia. *Bulletin of the Hungarian Geological Society*, **137**, 193–227.

Dabi G, M. Tóth T, Schubert F (2009a) Carbonate veins of different texture and their role in reconstructing fracture cementation (Ófalu, Goldgrund valley). *Bulletin of the Hungarian Geological Society*, **139**, 3–20.

Dabi G, Schubert F, M. Tóth T (2009b) Application of fluid inclusions in antitaxial veins as a gauge of fluid pressure fluctuation during vein growth. ECROFI XX. Abstract series, pp. 59–60.

Etheridge MA, Wall VJ, Cox SF, Vernon RH (1984) High fluid pressures during regional metamorphism and deformation: implications for mass transport and deformation mechanisms. *Journal of Geophysical Research*, **89**, 4344–58.

Fourcade S, Michelot JL, Buschaert S, Cathelineau M, Freiberger R, Coulibaly Y, Aranyossy JF (2002) Fluid transfers at the basement/cover interface: Part I. Subsurface recycling of trace carbonate from granitoid basement rocks (France). *Chemical Geology*, **192**, 99–119.

Friedman I, O'Neil JR (1977) Compilation of stable isotope fractionation factors of geochemical interest. In: *Data of Geochemistry*, 6th edn (ed. Fleischer M), Chapter KK. USGS Professional Papers 440-KK.

Fülöp J (1994) *Geology of Hungary, Paleozoic II (in Hungarian)*, pp. 297–306. Akadémiai Kiadó, Budapest.

Goldstein RH, Reynolds TJ (1994) *Systematics of Fluid Inclusions in Diagenetic Minerals. SEPM Short Course*, Vol. 31. Society of Economic Paleontologists and Mineralogists, Tulsa.

Haas J, Péró Cs (2004) Mesozoic evolution of the Tisza Mega-unit. *International Journal of Earth Sciences (Geologische Rundschau)*, **93**, 297–313.

Harangi S (1994) Geochemistry and petrogenesis of the Early Cretaceous continental rift-type volcanic rocks of the Mecsek Mountains, South Hungary. *Lithos*, **33**, 303–21.

Hilgers C, Sindern S (2005) Textural and isotopic evidence on the fluid source and transport mechanism of antitaxial fibrous microstructures from the Alps and the Appalachians. *Geofluids*, **5**, 239–50.

Hilgers C, Urai JL (2002a) Microstructural observations on natural syntectonic fibrous veins: implications for the growth process. *Tectonophysics*, **352**, 257–74.

Hilgers C, Urai JL (2002b) Experimental study of syntaxial vein growth during lateral fluid flow in transmitted light: first results. *Journal of Structural Geology*, **24**, 1029–43.

Hilgers C, Dilg-Gruschinski K, Urai JL (2003) Microstructures grown experimentally from advective supersaturated solution and their implication for natural vein systems. *Journal of Geochemical Exploration*, **78–79**, 221–5.

Hilgers C, Urai JL (2005) On the arrangement of solid inclusions in fibrous veins and the role of the crack-seal mechanism. *Journal of Structural Geology*, **27**, 481–94.

Hilgers C, Koehn D, Bons PD, Urai JL (2001) Development of crystal morphology during unitaxial growth in a progressively widening vein: II. Numerical simulations of the evolution of antitaxial fibrous veins. *Journal of Structural Geology*, **23**, 873–85.

Juhász A, M. Tóth T, Ramseyer K, Matter A (2002) Connected fluid evolution in fractured crystalline basement and overlying sediments, Pannonian Basin, SE Hungary. *Chemical Geology*, **182**, 91–120.

Kandori K, Sakai J, Ishikawa T (2000) Definitive effects of chloride ions on the formation of spherical hematite particles in a forced hydrolysis reaction. *Physical Chemistry Chemical Physics*, **2**, 3293–9.

Kandori K, Yamamoto N, Yasukawa A, Ishikawa T (2002) Preparation and characterization of disk-shaped hematite particles by a forced hydrolysis reaction in the presence of polyvinyl alcohol. *Physical Chemistry Chemical Physics*, **4**, 6116–22.

Király E, Koroknai B (2003) The magmatic and metamorphic evolution of the north-eastern part of the Mórágy Block. In: *Annual Report of the Geological Institute of Hungary 2003 (2004)*, pp. 299–318.

Kovács S, Szederkényi T, Haas J, Buda Gy, Császár G, Nagymarosy A (2000) Tectonostratigraphic terranes in the pre-Neogene basement in the Hungarian part of the Pannonian area. *Acta Geologica Hungarica*, **43**, 225–328.

Kovács-Pálffy P, Földvári M (2003) Hydrothermal minerals and phenomena in the Mórágy Granite Formation. In: *Annual Report of the Geological Institute of Hungary 2003* (ed. Balla Z), pp. 319–31.

Lassey KR, Blattner P (1988) Kinetically controlled oxygen isotope exchange between fluid and rock in one-dimensional advective flow. *Geochimica et Cosmochimica Acta*, **52**, 2169–75.

Lee Y-J, Morse JW (1999) Calcite precipitation in synthetic veins: implications for the time and fluid volume necessary for vein filling. *Chemical Geology*, **156**, 151–70.

Lee Y-J, Morse JW, Wiltsko DV (1996) An experimentally verified model for calcite precipitation in veins. *Chemical Geology*, **130**, 203–15.

Lelkes-Felvári Gy, Árkai P, Frank W, Nagy G (2000) Late Variscan ultramylonite from the Mórágy Hills, SE Mecsek Mts., Hungary. *Acta Geologica Hungarica*, **43**, 65–84.

Lespinasse M (1999) Are fluid inclusion planes useful in structural geology? *Journal of Structural Geology*, **21**, 1237–43.

Morris RV, Ming DW, Graff TG, Arvidson RE, Bell JF III, Squyres SW, Mertzman SA, Gruener JE, Golden DC, Le L, Robinson GA (2005) Hematite spherules in basaltic tephra altered under aqueous, acid-sulfate conditions on Mauna Kea volcano, Hawaii: possible clues for the occurrence of hematite rich spherules in the Burns formation at Meridiani Planum, Mars. *Earth and Planetary Science Letters*, **240**, 168–78.

Némedi Varga Z (1998) Stratigraphy of the Jurassic formations of the Mecsek and the Villány units. In: *Stratigraphy of the Hungarian geological formations* (ed. Bérczy I, in Hungarian), pp. 319–36. Geological Institute of Hungary, MOL Hungarian Oil and Gas Company, Budapest.

Northrop DA, Clayton RN (1966) Oxygen-isotope fractionations in systems containing dolomite. *The Journal of Geology*, **74**, 174–96.

O'Neil JR, Clayton NR, Mayeda TK (1969) Oxygen isotopic fractionation in divalent metal carbonates. *The Journal of Chemical Physics*, **51**, 5547–58.

Parry WT (1998) Fault-fluid compositions from fluid-inclusion observations and solubilities of fracture-sealing minerals. *Tectonophysics*, **290**, 1–26.

Poros ZS, Molnár F, Koroknai B, Lespinasse M, Maros Gy, Benkó Zs (2008) Application of studies on fluid inclusion planes and fracture systems in the reconstruction of the fracturing history of granitoid rocks III: results of studies in drillcores from the radioactive waste depository site at Bátaapáti (Üveghuta). *Bulletin of the Hungarian Geological Society*, **138/4**, 361–82.

Prokoph A, Shields GA, Veizer J (2008) Compilation and time-series analysis of a marine carbonate $\delta^{18}O$, $\delta^{13}C$, $^{87}Sr/^{86}Sr$ and $\delta^{34}S$ database through Earth history. *Earth-Science Reviews*, **87**, 113–33.

Ramsay JG (1980) The crack-seal mechanism of rock deformation. *Nature*, **284**, 135–9.

Raucsik B (1997) Stable isotopic composition of the Komló Calcareous Marl Formation ("Spotted Marl" s. str.), Mecsek Mountains, S Hungary. *Acta Mineralogica-Petrographica, Szeged*, **38**, 95–109.

Rye DM, Bradbury HJ (1988) Fluid flow in the crust: an example from a Pyrenean thrust ramp. *American Journal of Science*, **288**, 197–235.

Schubert F, Diamond LW, M. Tóth T (2007) Fluid-inclusion evidence of petroleum migration through a buried metamorphic dome in the Pannonian Basin, Hungary. *Chemical Geology*, **244**, 357–81.

Sibson RH (1998) Brittle failure mode plots for compressional and extensional tectonic regimes. *Journal of Structural Geology*, **20**, 655–60.

Szabó B, Benkó Zs, Molnár F (2008) The application of studies on fluid inclusion planes and fracture systems in the reconstruction of fracturing history of granitoid rocks II. Fracture systems of the Mórágy Granite. *Bulletin of the Hungarian Geological Society*, **138**, 193–227.

Taylor BE (1987) Stable isotope geochemistry of ore forming fluids. In: *Short Course in Stable Isotope Geochemistry of Low Temperature Fluids*, Vol. 13. (ed. Kyser TK), Chap. 8, pp. 337–418. Mineralogical Association of Canada, Saskatoon.

Templeton AS, Chamberlain CP, Koons PO, Craw D (1998) Stable isotopic evidence for mixing between metamorphic fluids and surface-derived waters during recent uplift of the Southern Alps, New Zealand. *Earth and Planetary Science Letters*, **154**, 73–92.

Török Á (1998) Stratigraphy of the Triassic formations of the Mecsek and the Villány units. In: *Stratigraphy of the Hungarian Geological Formations* (ed. Bérczy I, in Hungarian), pp. 253–79. Geological Institute of Hungary, MOL Hungarian Oil and Gas Company, Budapest.

M. Tóth T, Szűcs É, Schubert F, Hollós Cs (2004) Conceptual fracture network model of the crystalline basement of the Szeghalom Dome (Pannonian Basin, SE Hungary). *Acta Geologica Hungarica*, **47/1**, 19–34.

M. Tóth T, Kovács G, Schubert F, Dályai V (2005) Origin and deformation history of the Ófalu migmatite. *Bulletin of the Hungarian Geological Society*, **135**, 331–52.

Twiss RJ, Moores E (1992) *Structural Geology*, 532 pp. W.H. Freeman, New York.

Varga A, Raucsik B, Hámorné Vidó M, Rostási Á (2007) Isotope geochemistry and characterization of hydrocarbon potential of black shale from Óbánya Siltstone Formation. *Bulletin of the Hungarian Geological Society*, **137**, 449–72.

Varga A, Mikes T, Raucsik B (2009) The petrography and heavy minerals of the Toarcian black shale of the Réka Valley section of the Mecsek Hills: a pilot study. *Bulletin of the Hungarian Geological Society*, **139**, 33–54.

Watson BE (1996) Surface enrichment and trace element uptake during crystal growth. *Geochimica et Cosmochimica Acta*, **60**, 5013–20.

Watson BE (2004) A conceptual model for near-surface kinetic controls on the trace element and stable isotope composition of abiogenic calcite crystals. *Geochimica et Cosmochimica Acta*, **68**, 1473–88.